Energy Science & Engineering

WILEY

ORIGINAL ARTICLE OPEN ACCESS

Fault Detection and Classification in Five-Level Reduced Device Count Multilevel Inverter Using Fuzzy Logic System

Niraj Kumar Dewangan[1] | Jeevan N. D.[1] | Krishna Kumar Gupta[2] | Abhinandan Routray[1] | Hani Vahedi[3]

[1]Manipal Institute of Technology, Manipal Academy of Higher Education, Manipal, India | [2]Department of Electrical and Instrumentation Engineering, Thapar Institute of Engineering and Technology, Patiala, Punjab, India | [3]Electrical Sustainable Energy Department, Delft University of Technology, Delft, the Netherlands

Correspondence: Niraj Kumar Dewangan (niraj.dewangan@manipal.edu)

Received: 28 October 2025 | **Revised:** 23 March 2026 | **Accepted:** 7 April 2026

Funding: Manipal Academy of Higher Education, Manipal

Keywords: electric vehicle | fuzzy logic | multilevel inverter | open circuit faults | renewable energy

ABSTRACT

The reliable performance of multilevel inverters (MLIs) is critical to the advancement of power electronic systems used in renewable energy conversion, microgrid operation, and electric vehicle technologies. However, these systems are often susceptible to open-circuit faults in power switches, which can adversely affect output waveform quality and overall system stability if not detected early. This study presents an intelligent fault detection and localization strategy based on a fuzzy inference system (FIS) for a reduced device count cross-connected-source MLI. The proposed diagnostic framework employs output voltage and current signals as diagnostic parameters, enabling precise identification of fault conditions. A comprehensive set of fuzzy rules is developed to differentiate between single and double switch faults under diverse fault inception angles. Real-time validation is carried out using the dSPACE DS1202 controller in a hardware-in-the-loop environment. The findings confirm that the proposed FIS-based approach achieves high fault classification accuracy, rapid response time, and strong adaptability across varying operating conditions, highlighting its suitability for real-time condition monitoring in modern power conversion systems.

1 | Introduction

The cross-connected-source multilevel inverter (CCS-MLI) introduces a modern approach to power conversion that effectively bridges performance and simplicity. Unlike traditional cascaded H-bridge or neutral-point-clamped configurations, the CCS-MLI achieves comparable or superior output quality using fewer direct current (DC) sources and switching devices, leading to reduced system cost and improved reliability [1, 2]. The distinctive cross-connected DC source layout enables the production of multiple voltage levels without relying on separate isolated supplies for each stage, simplifying hardware and control requirements. This topology not only enhances power conversion efficiency but also minimizes total harmonic distortion, contributing to cleaner and more stable power delivery. Its ability to accommodate both symmetric and asymmetric voltage configurations further broadens its applicability in renewable energy systems, electric vehicles, and medium-voltage industrial drives [3–5]. The cross-connected arrangement, while reducing the overall component count, can also introduce challenges such as component failures, particularly in switching devices, a common issue in topologies involving a large number of power switches. Basically, two types of faults occur in power semiconductor switches: open-circuit faults (OCFs) and short-circuit faults (SCFs). SCFs are highly time-critical and must be identified within microseconds. Such fast fault detection and

exclusion (FDE) is typically handled by hardware protection circuits. Therefore, this paper mainly focuses on OCFs in single and multiple switch failures. These issues are dangerous to the healthy components and even to the entire system. The on-time monitoring and FDE are necessary in this respect. In the existing literature [6, 7], researchers have presented many methods to detect and diagnose OCFs, including model-, signal-processing-, and data-based techniques.

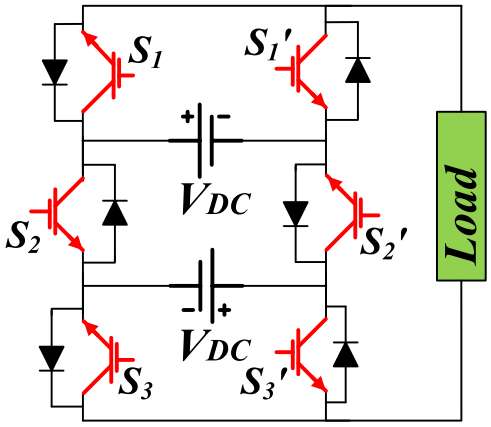

FIGURE 1 | Five-level cross-connected-source multilevel inverter topology. DC, direct current.

TABLE 1 | Specifications for the proposed CCS-MLI.

Parameters	Specifications
Input voltage (V_{DC}) (V)	20
Load (R) (Ω)	40
System frequency (Hz)	50
Switching frequency (Hz)	1000
Modulation index	0.85

Abbreviations: CCS-MLI, cross-connected-source multilevel inverter; DC, direct current.

Model-based fault diagnosis and isolation (FDI) techniques for multilevel converters have been the focus of significant research in recent years. These approaches generally rely on developing mathematical representations of normal system behavior and identifying deviations between predicted and measured responses to detect and isolate faults [8]. For instance, Wassinger et al. [9] proposed a state-space observer-based approach for FDE in interleaved power converters. The method accurately identifies the affected phase and maintains reliable FDE efficiency even under modeling uncertainties and measurement noise. In a similar direction, Xu et al. [10] developed an observer-driven scheme for FDE and isolation in current and DC-link voltage sensors. This technique employs residual signals derived from both observer estimations and measured quantities, with its robustness and stability verified through analytical validation. Furthermore, Jlassi et al. [11] presented a diagnostic framework capable of distinguishing single faults among multiple IGBT OCFs and current sensor malfunctions in permanent-magnet synchronous motor drives. The approach utilizes residuals from observed and measured stator currents, incorporating an adaptive threshold to ensure dependable FDE across diverse operating conditions. Another contribution, reported in [12], introduced a Luenberger observer-based diagnostic system that compares measured and estimated inductor currents. When the deviation exceeds an adaptive threshold, an OCF is accurately identified, ensuring prompt and reliable fault indication.

Signal-processing-based FDI techniques for MLIs have been extensively used in research. These methods focus on analyzing the inverter's output signals to detect and localize faults, such as open-circuit (OC) or short-circuit (SC) conditions in the power semiconductor switches. A method in [13] defines two types of eigenvalues based on voltage polarity in specific time zones. Envelope functions are used to classify faults based on whether abnormal conditions occur in corresponding time zones. Kalaiarasi et al. [14] utilize the output current waveform of a cascaded H-bridge MLI (CHB-MLI) for FDE, which identifies which switch failed based on timing and polarity. Another

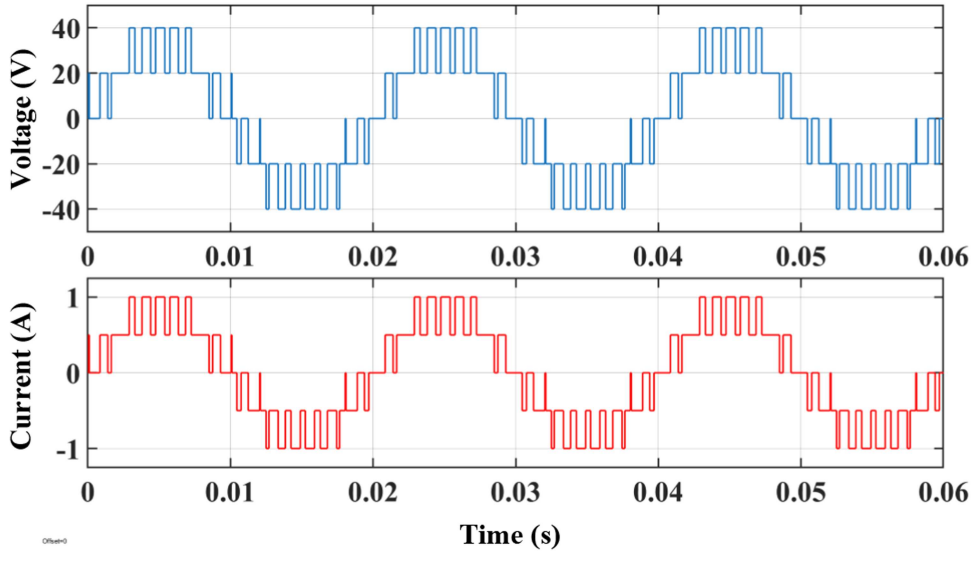

FIGURE 2 | The healthy output waveforms of the mentioned multilevel inverter.

TABLE 2 | Different faults and their classes of the CCS-MLI.

Class label	Types of faults	OCF location	Fault cases per class	DF voltage (healthy)	DF voltage (faulty)	DF current (healthy)	DF current (faulty)	Fault cases
1	Two switches	S'_2, S'_3	1	33.74	4.08	0.84	0.102	1
2	Two switches	S_1, S_2	1	33.74	5.8	0.84	0.144	2
3	Two switches	S_1, S'_3	1	33.74	9.86	0.84	0.246	3
4	Two switches	S'_1, S'_2	1	33.74	11.76	0.84	0.294	4
5	Two switches	S_2, S_3	1	33.74	12.12	0.84	0.303	5
6	Single switch	S'_2	4	33.74	15.83	0.84	0.396	6
	Two switches	S_1, S_3						7
		S_1, S'_2						8
		S_3, S'_2						9
7	Single switch	S_2	4	33.74	17.91	0.84	0.44	10
	Two switches	S_2, S'_1						11
		S_3, S'_2						12
		S'_1, S'_3						13
8	Single switch	S_1	2	33.74	21.98	0.84	0.549	14
		S'_3						15
9	Two switches	S_3, S'_1	1	33.74	23.88	0.84	0.597	16
10	Single switch	S_3	1	33.74	29.23	0.84	0.741	17
11	Single switch	S'_1	1	33.74	30.1	0.84	0.784	18

Abbreviations: CCS-MLI, cross-connected-source multilevel inverter; DF, discrete Fourier; OCF, open-circuit fault.

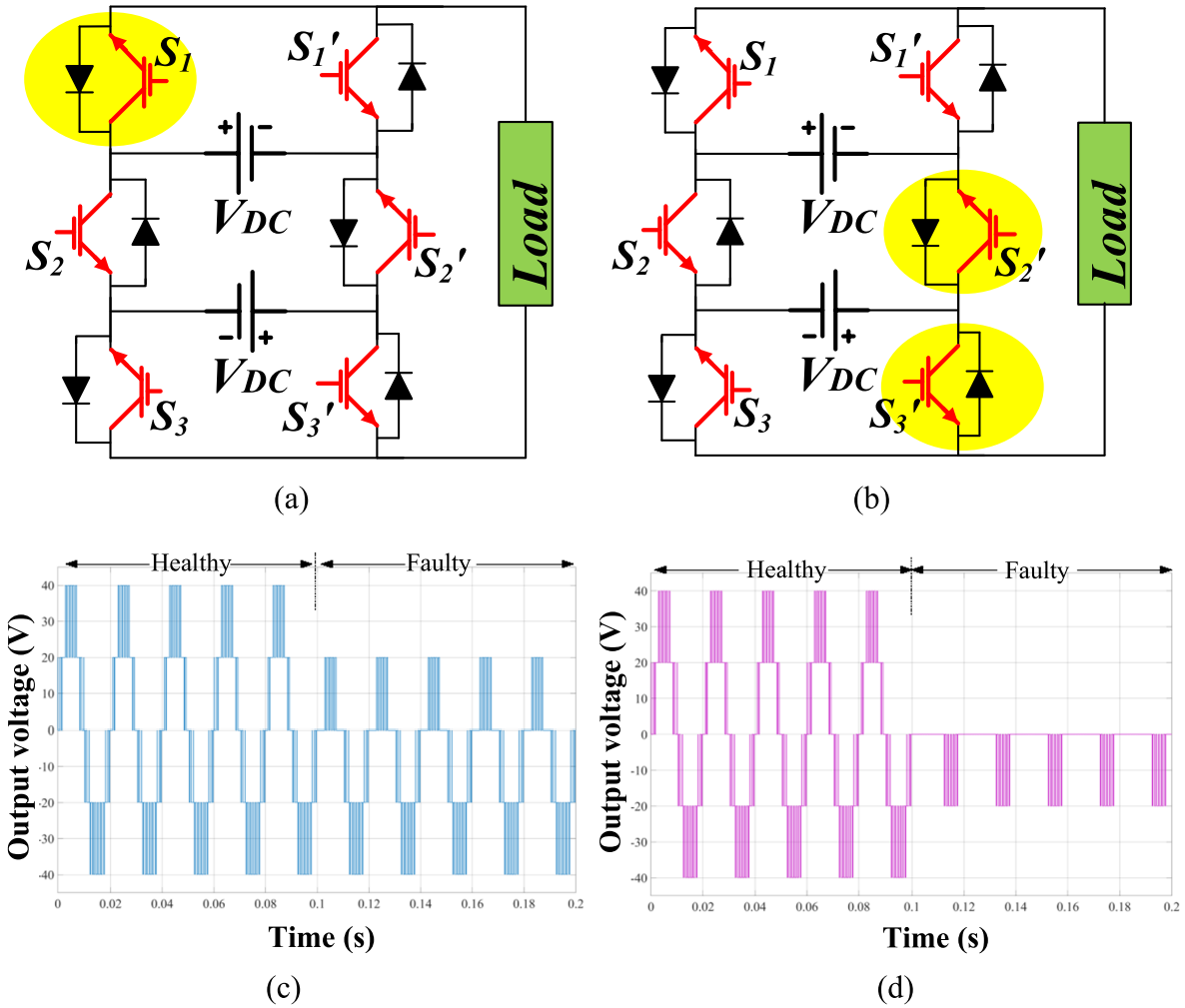

FIGURE 3 | CCS-MLI topology showing (a) OCF at S_1, (b) OCF at S_2' and S_3', with corresponding output voltage waveforms (c, d). CCS-MLI, cross-connected-source multilevel inverter; DC, direct current; OCF, open-circuit fault.

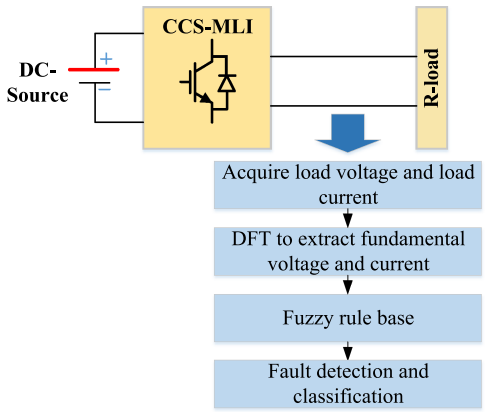

FIGURE 4 | Block diagram showing FDE and classification methodology. CCS-MLI, cross-connected-source multilevel inverter; DC, direct current; DFT, discrete Fourier transform; FDE, fault detection and exclusion.

signal-based detection method to diagnose OCFs in individual IGBT switches of CHB-MLI was proposed in [15].

Data-based approaches utilize mathematical techniques for FDE and identification. Unlike model-based and signal-based methods, data-driven approaches do not depend on the system model, load conditions, or signal characteristics. These methods are relatively easy to implement and operate independently of varying operational conditions; their performance relies on historical data and machine learning (ML) algorithms [16]. A key limitation is that it requires a large amount of data to train an ML algorithm. The important steps involved before feeding data as ML input are feature extraction and data preprocessing. The extraction of features from the signal is a crucial step; otherwise, misclassification may take place. In the preprocessing step, the unwanted data may be removed. In [17], many ML algorithms, including support vector machine (SVM) and decision trees (DTs), are used for classifying the faults; however, the classification time is not shown. Similarly, several ML methods are studied in the literature [18, 19] to diagnose OCFs and SCFs. In most cases, authors executed offline FDI. Also, some authors [20, 21] have applied deep learning (DL) techniques for OCF diagnosis.

Recent studies have increasingly adopted hybrid FDI approaches that combine signal processing with artificial intelligence (AI) for MLIs [22–25]. These methods combine feature extraction from raw electrical signals with ML or DL classifiers, such as neural networks with joint approximate diagonalization of eigen-matrices-independent component analysis processed

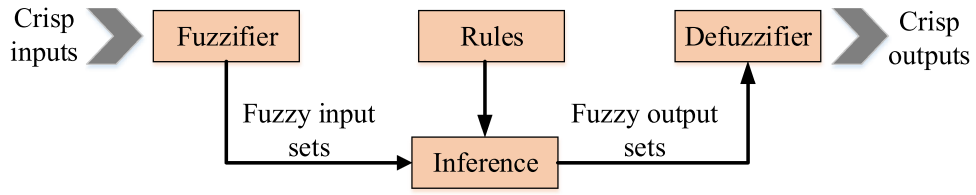

FIGURE 5 | Block diagram of the fuzzy logic system.

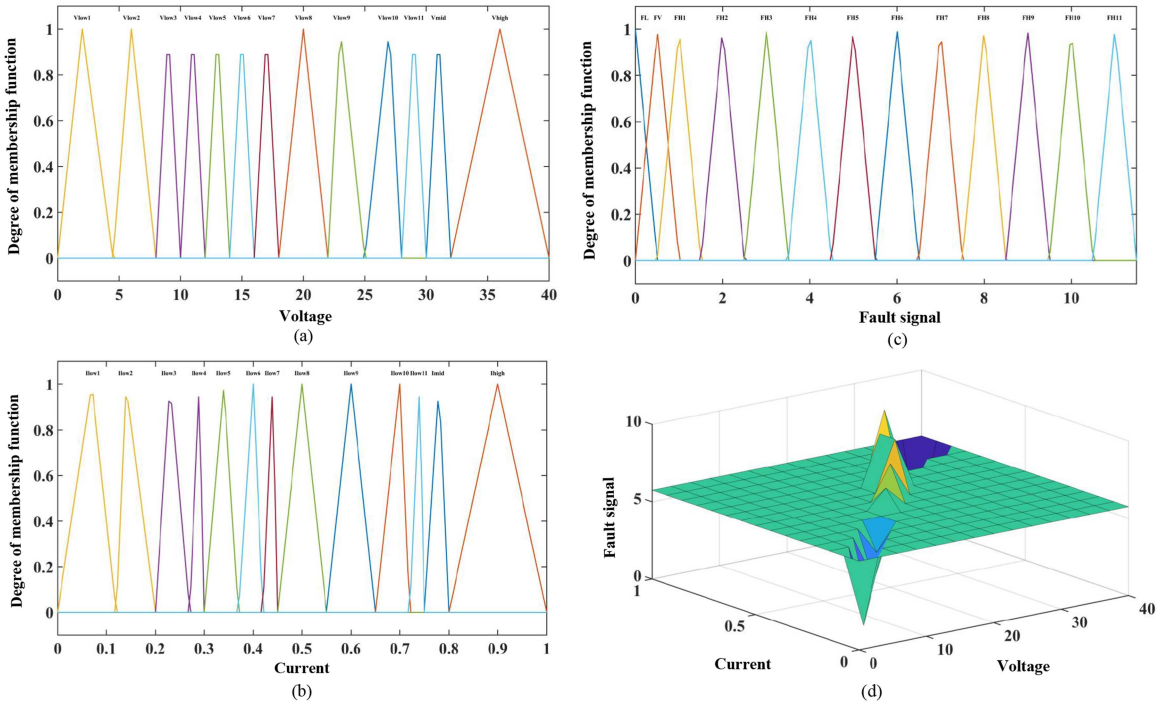

FIGURE 6 | The FDI and classification: (a) DF voltage membership function (MF), (b) DF current MFs, (c) output MF, and (d) the surface viewer of fuzzy rules. DF, discrete Fourier; FDI, fault diagnosis and isolation.

TABLE 3 | Fault recognition based on fuzzy logic rule.

Fuzzy logic rule			
Parameters	V_{Low} (V_L)	V_{Mid} (V_M)	V_{High} (V_H)
I_{Low} (I_L)	F_H	F_L	F_L
I_{Mid} (I_M)	F_L	F_V	F_L
I_{High} (I_H)	F_L	F_L	F_L

Note: F_H = fault signal high, F_L = fault signal low, and F_V = fault signal in verge condition.

voltage signals [22], SVMs using wavelet-based entropy features [23], discrete wavelet transform (DWT) based features with ML classifiers for packed U-cell 5 (PUC-5) inverters [24], and a wavelet packet transform combined with long short-term memory networks [25], have been applied for OCF detection and localization.

Fuzzy logic systems (FLSs), a knowledge-based method, are infrequently employed for the detection and classification of switch faults. In [26], DWT is used to decompose the voltage waveform into approximations and detailed coefficients. Detailed coefficients from all cases (faulty and healthy) are collected and used as input for FLS. In [27], FDE and isolation are performed using an FLS in modular multilevel converters (MMCs). Another study [28] used discrete Fourier (DF) voltage and current as input to FLS for OCF detection and classification in a CHB inverter. FLS offers an attractive solution in power electronics due to its simple design process, effective handling of system nonlinearities, and minimal requirement for deep system knowledge. This paper focuses on OCF (in single switch and two switches) detection and classification in a five-level CCS-MLI topology. Simulations of the MLI under normal and fault scenarios are carried out using MATLAB/Simulink.

The paper is structured as follows: Section 2 presents the proposed topology and outlines the characteristics of OCFs in CCS-MLI. Section 3 discusses the fuzzy logic-based FDE and classification approach. Section 4 provides a comprehensive evaluation of FDE and classification under various fault conditions and a detailed comparative analysis. Finally, Section 5 concludes the paper by summarizing the key findings.

2 | Description and Analysis of the MLI Structure

A five-level CCS-MLI topology has been taken for this work to investigate OCFs in semiconductor switches. The inverter topology and associated switch signal generation methods are

TABLE 4 | FC-based fuzzy logic rule.

Parameters	V_H	V_M	V_{L1}	V_{L2}	V_{L3}	V_{L4}	V_{L5}	V_{L6}	V_{L7}	V_{L8}	V_{L9}	V_{L10}	V_{L11}
I_H	F_L	F_L	F_L	F_L	F_L	F_L	F_L	F_L	F_L	F_L	F_L	F_L	F_L
I_M	F_L	F_V	F_L	F_L	F_L	F_L	F_L	F_L	F_L	F_L	F_L	F_L	F_L
I_{L1}	F_L	F_L	F_{H1}	F_L	F_L	F_L	F_L	F_L	F_L	F_L	F_L	F_L	F_L
I_{L2}	F_L	F_L	F_L	F_{H2}	F_L	F_L	F_L	F_L	F_L	F_L	F_L	F_L	F_L
I_{L3}	F_L	F_L	F_L	F_L	F_{H3}	F_L	F_L	F_L	F_L	F_L	F_L	F_L	F_L
I_{L4}	F_L	F_L	F_L	F_L	F_L	F_{H4}	F_L	F_L	F_L	F_L	F_L	F_L	F_L
I_{L5}	F_L	F_L	F_L	F_L	F_L	F_L	F_{H5}	F_L	F_L	F_L	F_L	F_L	F_L
I_{L6}	F_L	F_L	F_L	F_L	F_L	F_L	F_L	F_{H6}	F_L	F_L	F_L	F_L	F_L
I_{L7}	F_L	F_L	F_L	F_L	F_L	F_L	F_L	F_L	F_{H7}	F_L	F_L	F_L	F_L
I_{L8}	F_L	F_L	F_L	F_L	F_L	F_L	F_L	F_L	F_L	F_{H8}	F_L	F_L	F_L
I_{L9}	F_L	F_L	F_L	F_L	F_L	F_L	F_L	F_L	F_L	F_L	F_{H9}	F_L	F_L
I_{L10}	F_L	F_L	F_L	F_L	F_L	F_L	F_L	F_L	F_L	F_L	F_L	F_{H10}	F_L
I_{L11}	F_L	F_L	F_L	F_L	F_L	F_L	F_L	F_L	F_L	F_L	F_L	F_L	F_{H11}

Note: F_H = fault signal high, F_L = fault signal low, and F_V = fault signal in verge condition.

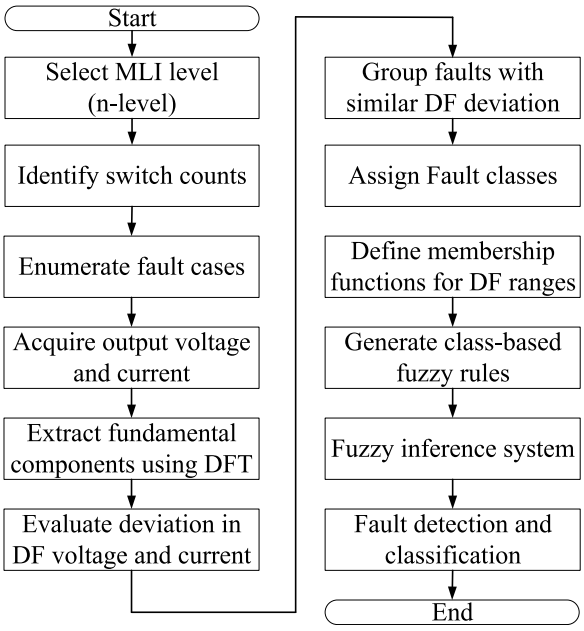

FIGURE 7 | Generalized DFT-based framework for n-level MLIs. DF, discrete Fourier; DFT, discrete Fourier transform; MLI, multilevel inverter.

discussed in detail. A subsequent subsection discusses the effects of OCFs on the inverter output ac voltage and takes into account various combinations of OCFs.

2.1 | Five-Level CCS-MLI

Figure 1 shows the topology of a five-level CCS-MLI [29]. The CCS-MLI uses floating and isolated DC sources. The sources are connected alternately in opposite polarities using complementary switch pairs. Each voltage source contributes individually or in combination to the output voltage. This configuration enables $2n + 1$ voltage levels using only $2n + 2$ switches, where n is the number of DC sources. For 2 sources ($n = 2$), we get a five-level output: $-2V_{DC}, -V_{DC}, 0, +V_{DC}, +2V_{DC}$ and the switches are S_1, S_2, S_3 and corresponding complementary switches are shown in Figure 1. The parameters chosen for the analysis are shown in Table 1.

2.2 | Modulation Strategy

A level-shifted pulse width modulation strategy [30] is employed to control the switching of devices and synthesize the desired stepped output waveform. The modulation scheme uses four triangular carrier signals arranged in phase disposition configuration, which are compared with a 50-Hz sinusoidal reference waveform. The generated aggregated signal is fed to OR-gates to produce switching pulses to semiconductor switches. Figure 2 shows the waveforms of the output voltage and current for the presented topology.

2.3 | OCF Analysis of Five-Level CCS-MLI

In this work, faults that occur due to the OC of either a single switch or two switches have been studied. In the five-level CCS-MLI, 18 possible OC single-switch and two-switch faults are taken for fault analysis. All these possible combinations of faults are divided into 11 classes depending upon the deviation of the magnitude of the fundamental component of voltage measured using the discrete Fourier transform (DFT), as illustrated in Table 2.

Several cases of OCF conditions on switches have been simulated to study the output characteristics of CCS-MLI. In Figure 3a,b, the topology of the CCS-MLI highlighting fault at S_1, S_2', and S_3', and in Figure 3c,d shows the corresponding output voltage waveforms, respectively. For instance, an OCF is created on a switch S_1, at $t = 0.1$s, the waveform in Figure 3c consists of only one level of +20 V in the positive half cycle and two levels of −20 and −40 V in the negative half cycle, resulting in a loss of some voltage levels due to OCF at switch S_1. In the second example, a fault is created on switches S_2' and S_3', the output voltage waveform is distorted after a fault is created

TABLE 5 | Details of findings of fuzzy-based FDE and classification for CCS-MLI.

Class	Fault types	Fault modes (OC)	FDE time (ms)	FC time (ms)	Output cases
1	Two switches	S_2', S_3'	4	20	1
2	Two switches	S_1, S_2	5	19	2
3	Two switches	S_1, S_3'	5	20	3
4	Two switches	S_1', S_2'	7	20	4
5	Two switches	S_2, S_3	4	17	5

Abbreviations: CCS-MLI, cross-connected-source multilevel inverter; FC, fault classification; FDE, fault detection and exclusion; OC, open circuit.

at $t = 0.1$s, as illustrated in Figure 3d. In this case, in the positive half cycle, no voltage levels are present, and in the negative half cycle only one voltage level, that is, −20 V exists.

Further, various OCF case studies have been considered and listed in Table 2. From Figure 3, it can be concluded that whenever a fault occurs on any of the switches of CCS-MLI, the output voltage would be distorted. Also, there will be a loss of some levels in the voltage waveform. Thus, there will be a clear distinction between healthy and faulty conditions. By utilizing these distinct changes, a fuzzy-based FDE and classification methodology has been developed in Section 3.

3 | Proposed Fuzzy-Based FDE and Classification Technique

As discussed in Section 2, the output voltage and current exhibit distinct behaviors under healthy and faulty conditions. Therefore, these signals can be effectively utilized to detect the presence of an OCF and identify the specific switch(es) that are open-circuited. In this work, as shown in Figure 4, both output voltage and output current signals of CC-MLI are preprocessed using DFT to get important features from the voltage and current. These are then fed to the fuzzy system. The fuzzy-based system generates the FDE signal and provides the class that the particular case fall. There is a total of 11 classes, each representing different fault locations. The FLS mainly consists of membership functions (MFs), fuzzy rule base, and output, which is very efficient and fast compared with other detection techniques. There are basically two types of fuzzy logic controllers (FLCs): the Mamdani FLC and the Takagi-Sugeno FLC. The Mamdani FLC is more widely used than the Takagi-Sugeno FLC due to its advantages in interpretability and its rule-based decision-making structure.

3.1 | Block Diagram of FLS

Figure 5 illustrates the working of an FLS. It starts with crisp inputs, which are precise numerical values, being converted into fuzzy input sets by the fuzzifier. These fuzzy sets are then processed in the inference engine using a set of predefined rules that capture expert knowledge in the form of if-then statements. The inference engine produces fuzzy output sets, which represent results in a fuzzy form. Finally, the defuzzifier converts these fuzzy outputs back into crisp outputs that can be used in real-world applications. In this work, the crisp inputs correspond to the numerical values of the DFT-extracted fundamental components of output voltage and current. During fuzzification, each crisp input value is mapped to one or more triangular MFs ($V_{L1} - V_{L11}$, V_M, V_H for voltage and $I_{L1} - I_{L11}$, I_M, I_H for current) according to its magnitude, thereby converting the numerical measurements into fuzzy linguistic variables. After defuzzification, the resulting crisp output is a discrete numerical value that directly represents the fault class number, where Classes 1–11 correspond to the respective OCF conditions defined in Table 2.

3.2 | Open Circuit FDE and Classification Using FLS

While other AI techniques like neural networks or DT might perform better when large, structured data sets are available, fuzzy logic shines in areas where human-like reasoning, complex systems with unclear boundaries, and flexibility in handling imprecise data are key.

In this work, a DFT block plays an important role in measuring the voltage and changes in the voltage when a fault occurs. The fault might be a single switch or multiple switch faults; the fundamental component of the DFT output is observed and measured for the fault prediction. These features of DFT output for healthy and faulty conditions are used to categorize the different faults. To improve adaptability under varying operating conditions, the extracted DF voltage can be normalized to $\frac{V_{load}}{2V_{DC}}$ and DF current to $\frac{i_{load}}{i_{base}}$ $\left(i_{base} = \frac{2V_{DC}}{R}\right)$ before being applied to the fuzzy inference system. This normalization ensures that the input features are scaled within a consistent range, thereby reducing dependence on absolute voltage and current magnitudes. As a result, the proposed diagnostic framework is not strictly confined to a single operating point and can accommodate moderate variations in load or modulation conditions without requiring modification of the fuzzy rule base. This preprocessing step enhances the scalability and general applicability of the proposed method.

When an OCF occurs in switches S_2' and S_3', the DFT fundamental voltage drops from 33.7 to 4.08 V. According to Table 2, this condition corresponds to a Class 1 fault. Similarly, faults in other switching devices are categorized by evaluating the variations in DFT-based voltage and current parameters using the FLS, which accurately identifies the respective fault class.

Figure 6a,b illustrates the MFs for DF voltage and DF current used as inputs to the FLC, while Figure 6c,d shows the fault signal as the output of the FLS along with a 3D visualization of the inference rules. The FLS identifies faulty switches using DF-transformed voltage and current signals. Here, the MFs for

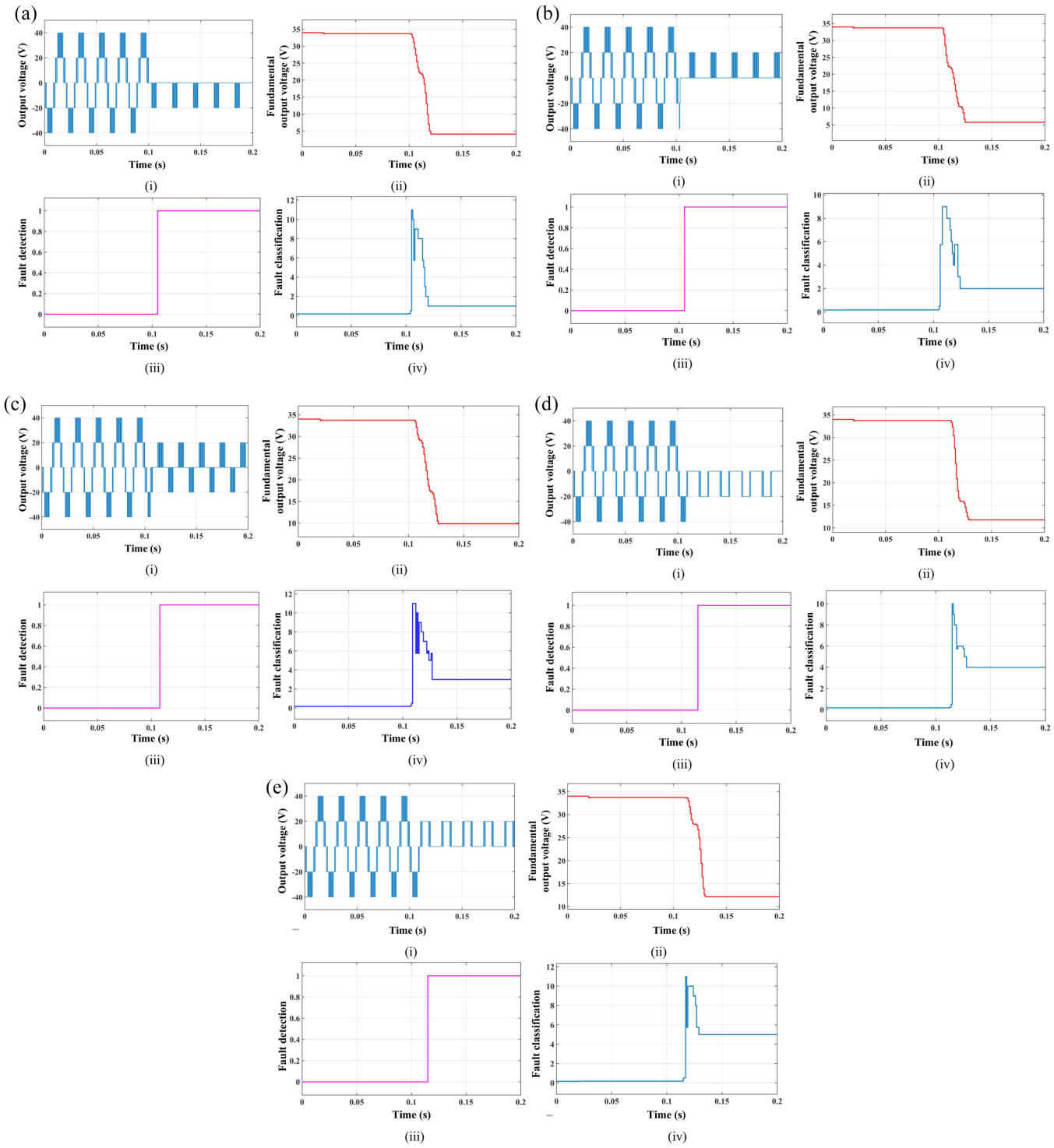

FIGURE 8 | (a) Different plots related to Class 1 fault when fault initiated at $t = 0.101$ s: (i) output voltage, (ii) DF output voltage, (iii) OCF detection, and (iv) OCF Classification. (b) Different plots related to Class 2 fault when fault initiated at t = 0.103 s: (i) output voltage, (ii) DF output voltage, (iii) OCF detection, and (iv) OCF classification. (c) Different plots related to Class 3 fault when fault initiated at $t = 0.105$ s: (i) output voltage, (ii) DF output voltage, (iii) OCF detection, and (iv) OCF classification. (d) Different plots related to Class 4 fault when fault initiated at $t = 0.107$ s: (i) output voltage, (ii) DF output voltage, (iii) OCF detection, and (iv) OCF classification. (e) Different plots related to Class 5 fault when fault initiated at $t = 0.109$ s: (i) output voltage, (ii) DF output voltage, (iii) OCF detection, and (iv) OCF classification. DF, discrete Fourier; OCF, open-circuit fault.

current and voltage are chosen to be triangular. The ranges for both inputs are divided into 13 ranges, that is, low1–11, middle-12, and high-13. The DF voltage range is divided into 13 fuzzy sets: 11 for the lower voltage levels, one for the medium level, and one for the higher voltage level, each represented by its own MF. Similarly, the DF current is also divided into fuzzy sets, with MFs assigned for different current ranges. Additionally, the output fault signal is represented by 13 MFs, which correspond to the ranges: one F_L, one F_V, and 11 levels from F_{H1} to F_{H11}. On the basis of the collected data of DF voltages and

TABLE 6 | Details of findings of fuzzy-based FDE and classification for CCS-MLI.

Class	Fault types	Fault modes (OC)	FDE time (ms)	FC time (ms)	Output cases
6	Single switch	S_2'	15	20	1
	Two switches	S_1, S_3			2
		S_1, S_2'			3
		S_3, S_2'			4
7	Single switch	S_2	4	10	5
	Two switches	S_2, S_1'			6
		S_3, S_2'			7
		S_1', S_3'			8

Abbreviations: CCS-MLI, cross-connected-source multilevel inverter; FC, fault classification; FDE, fault detection and exclusion; OC, open circuit.

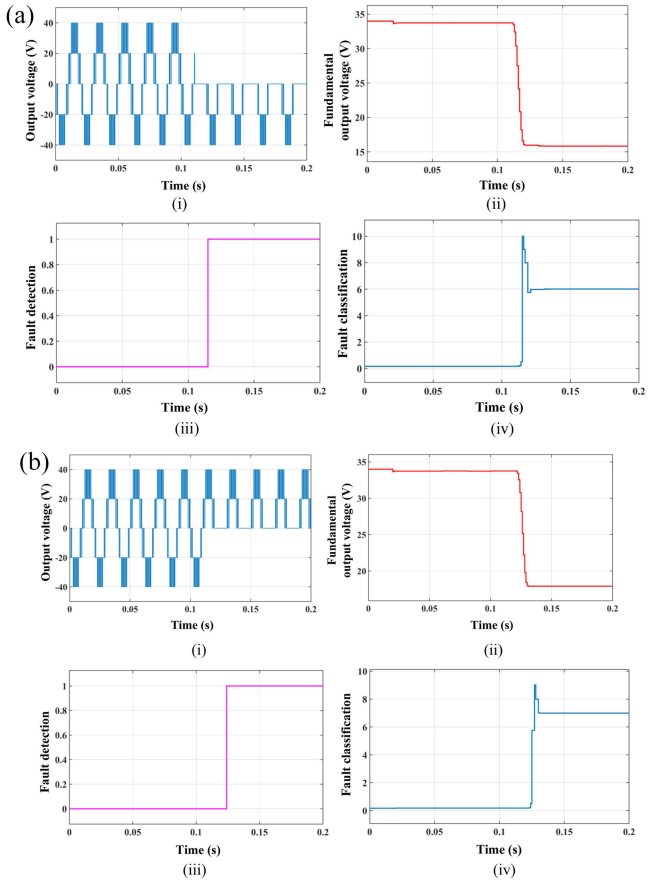

FIGURE 9 | (a) Different plots related to Class 6 fault when fault initiated at $t = 0.11$ s: (i) output voltage, (ii) DF output voltage, (iii) OCF detection, and (iv) OCF classification. (b) Different plots related to Class 7 fault when fault initiated at $t = 0.112$ s: (i) output voltage, (ii) DF output voltage, (iii) OCF detection, and (iv) OCF Classification. DF, discrete Fourier; OCF, open-circuit fault.

currents, rules are framed for all OCF conditions, including healthy conditions.

To ensure reproducibility, the MF breakpoints are selected in a data-driven manner based on the DF voltage and current magnitudes listed in Table 2. The boundaries between adjacent fuzzy regions are determined using midpoints between consecutive DF values corresponding to different fault classes, ensuring continuous but nonoverlapping coverage of the feature space. The fuzzy rule base is systematically derived by mapping each distinct (DF voltage and DF current) region to its corresponding fault class as defined in Table 2, rather than being manually tuned. The fault classification (FC) fuzzy rules are shown in Tables 3 and 4.

3.3 | Generalized FC Framework

Although the present work is demonstrated for a five-level CCS-MLI, the proposed diagnostic methodology is inherently scalable to higher-level MLIs. This scalability is achieved through the use of DFT-extracted fundamental voltage and current components as diagnostic features, which are independent of the inverter voltage level. For an n-level MLI, the number of switches and possible fault combinations increases; however, fault diagnosis is performed by grouping fault cases into classes based on similar deviations in DF voltage and current. As a result, the fuzzy inference structure and rule logic remain unchanged, while only the MF boundaries and class ranges are extended. The generalized flowchart in Figure 7 illustrates this systematic procedure for extending the proposed DFT-based fuzzy diagnostic framework to n-level MLIs without causing rule explosion.

4 | Simulation Results and Discussions

The platform used for simulations of the proposed diagnostic technique is MATLAB/Simulink toolbox. All the parameters used in the simulation are discussed in Table 1. The diagnostic system takes DF voltage and current as inputs and provides FC as the output. On the basis of predefined rules, the system classifies OCFs in switches. Different types of faults are simulated individually, as well as for two-switch faults. These faults are grouped into corresponding classes. All OCF cases are classified into 11 different classes based on FDE time, and the FLS evaluates for the classification of all faults according to the specific class the fault falls into. This section provides a detailed explanation of all types of OCFs, including both individual and multiple faults.

4.1 | Performance During Faults of Classes 1–5

As discussed in Table 2, there are 18 fault cases which include both single and two switch faults and 11 fault classes. Table 5 discusses five OCF cases at switches and corresponding fault classes. Here OCF at $S_2'S_3'$, S_1S_2, S_1S_3', $S_1'S_2'$, and $S_2S_3$with FDE

TABLE 7 | Details of findings of fuzzy-based FDE and classification for CCS-MLI.

Class	Fault types	Fault modes (OC)	FDE time (ms)	FC time (ms)	Output cases
8	Single switch	S_1	15	20	1
	Single switch	S_3'	4	11	2
9	Two switches	S_3, S_1'	8	17	3
10	Single switch	S_3	16	19	4
11	Single switch	S_1'	7	8	5

Abbreviations: CCS-MLI, cross-connected-source multilevel inverter; FC, fault classification; FDE, fault detection and exclusion; OC, open circuit.

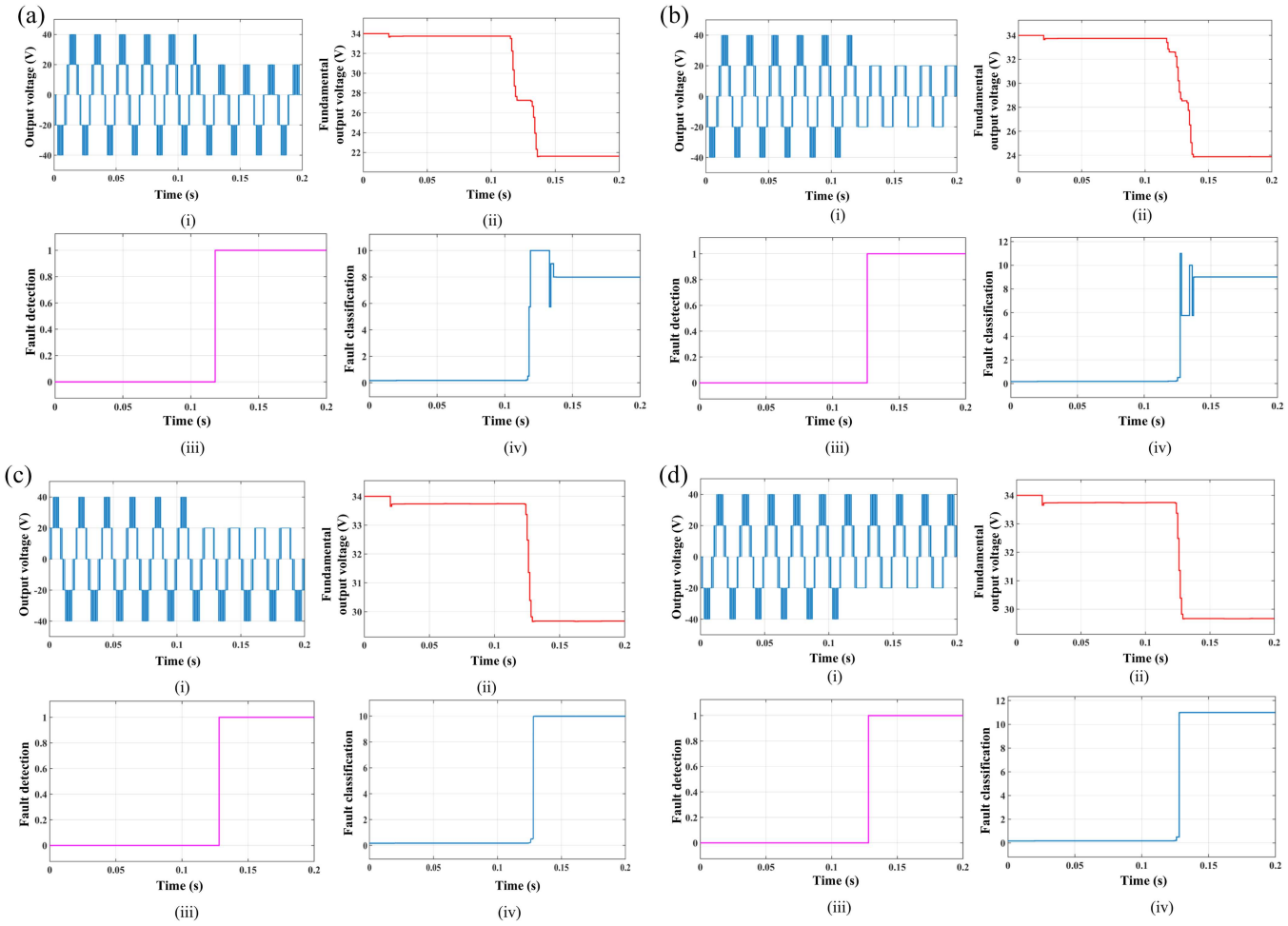

FIGURE 10 | (a) Different plots related to Class 8 fault when fault initiated at $t = 0.114$ s: (i) output voltage, (ii) DF output voltage, (iii) OCF detection, and (iv) OCF Classification. (b) Different plots related to Class 9 fault when fault initiated at $t = 0.116$ s: (i) output voltage, (ii) DF output voltage, (iii) OCF detection, and (iv) OCF Classification. (c) Different plots related to Class 10 fault when fault initiated at $t = 0.118$ s: (i) output voltage, (ii) DF output voltage, (iii) OCF detection, and (iv) OCF Classification. (d) Different plots related to Class 11 fault when fault initiated at $t = 0.12$ s: (i) output voltage, (ii) DF output voltage, (iii) OCF detection, and (iv) OCF Classification. DF, discrete Fourier; OCF, open-circuit fault.

and classification times are illustrated. Figure 8a–e consists of waveforms of output voltage, DF voltage waveform, OCF detection signal, and FC signal. For example, consider one case of OCF at switches $S_2'S_3'$ initiated at 0.101 s can be observed in Figure 8a(i), the output voltage is distorted after the fault occurrence. There is a change in DF voltage that can be observed in Figure 8a(ii), it changes from 33.74 to 4.08 V. These changes in the DF voltage are detected by FLS and trigger the fault signal. Figure 8a(iii) shows the FDE alert waveform, the detection signal suddenly changes from 0 to 1, where 0 indicates no fault and 1 indicates a fault has occurred. Once the fault is identified, FC is performed. The FC indicates where exactly the fault has occurred and the location of the fault (in which switch the fault occurred). Figure 8a(iv) shows the waveform of the classification of the fault at switches $S_2'S_3'$. The FLS took 20 ms to correctly classify the fault from the time of fault inception. The waveform is distorted when the fault is initiated. After 20 ms, the waveform settles to a value of one, indicating a fault of Class 1. Similarly, all fault cases are analyzed and shown in Figure 8b–e as tabulated in Table 5.

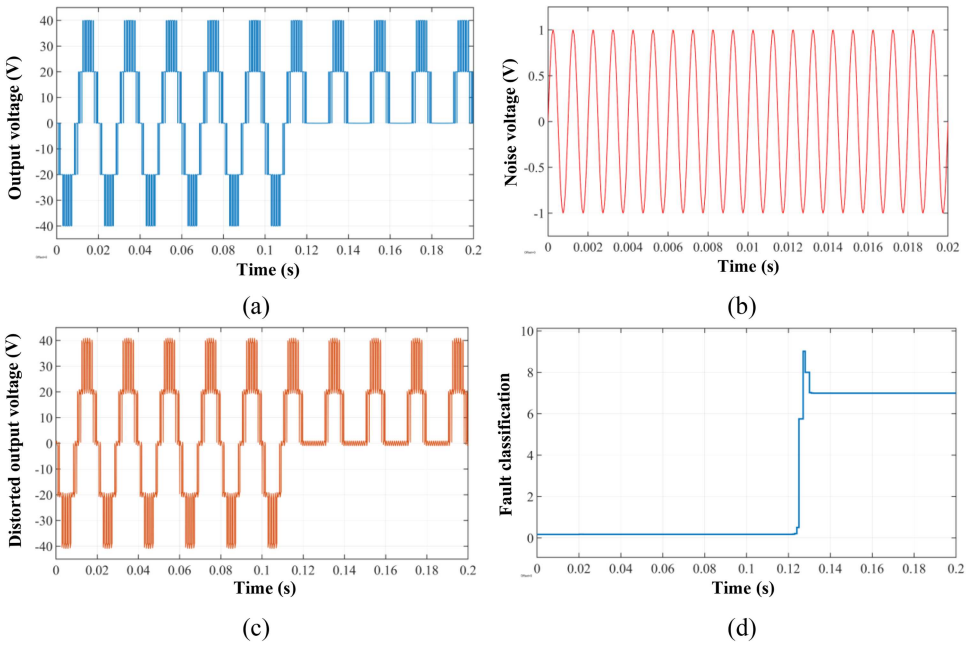

FIGURE 11 | Robustness evaluation under noisy voltage conditions: (a) original output voltage waveform for Class 7 fault initiated at $t = 0.112$ s, (b) injected high-frequency voltage noise (1 V, 1 kHz), (c) distorted output voltage after noise superposition, and (d) corresponding fault classification signal.

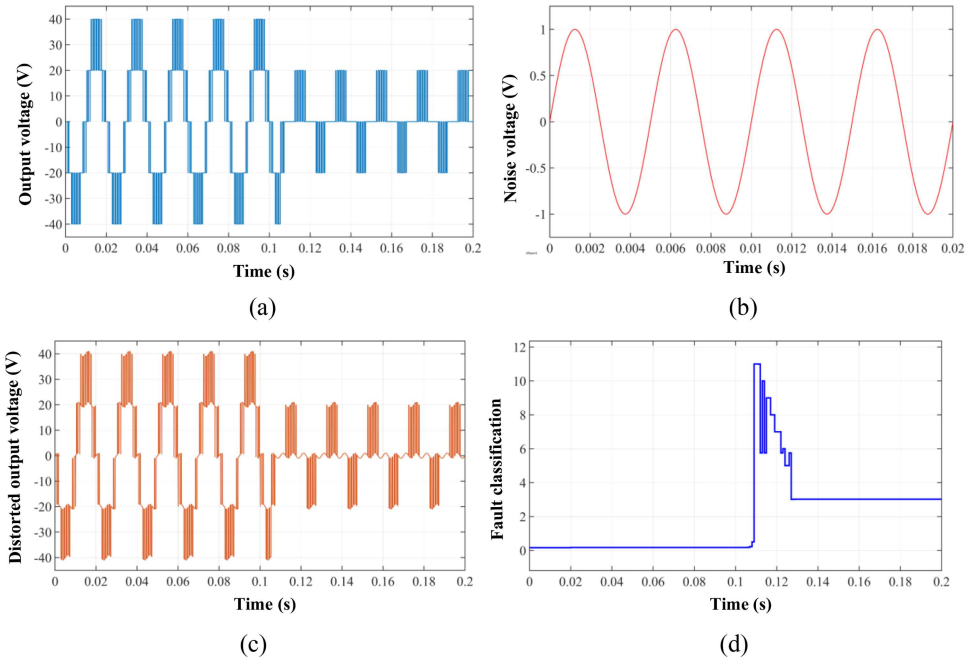

FIGURE 12 | Robustness evaluation under noisy voltage conditions: (a) original output voltage waveform for Class 3 fault initiated at $t = 0.105$ s, (b) injected low-frequency voltage noise (1 V, 200 Hz), (c) distorted output voltage after noise superposition, and (d) corresponding fault classification signal.

4.2 | Performance During Faults of Classes 6 and 7

The subsequent section extends the earlier discussion by examining eight distinct OCF scenarios, as outlined in Table 6. The first four cases, involving faults at switches

S_2', S_1S_3, S_1S_2', and S_3S_2' are categorized under Class 6. The remaining four cases, corresponding to OCF occurrences at switches S_2, S_2S_1', S_3S_2', and $S_1'S_3'$, are classified under fault Class 7. Figure 9a,b shows the output voltage waveform, DF voltage variation, FDE, and FC plots corresponding to fault Classes 6 and 7. For example, consider one case of OCF at S_2', initiated at 0.11 s, which can be observed in Figure 9a(i), the output voltage distorted after the fault occurrence. There is a change in DF voltage that can be observed in Figure 9a(ii), it changes from 33.74 to 15.83 V. These changes in the DF voltage are detected

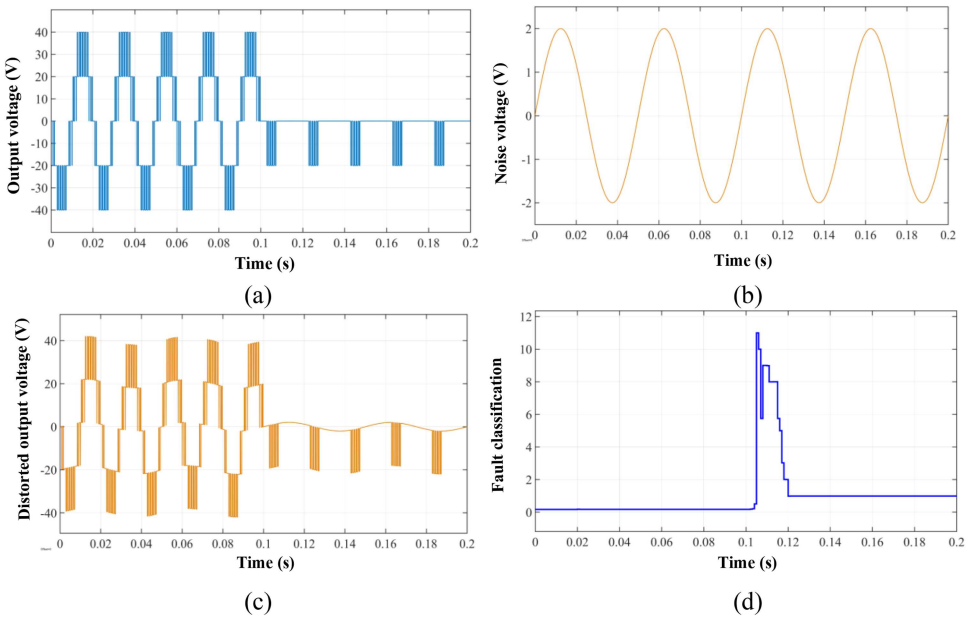

FIGURE 13 | Robustness evaluation under low-frequency noise conditions: (a) original output voltage waveform for Class 1 fault initiated at $t = 0.1$ s, (b) injected low-frequency voltage noise (2 V, 20 Hz), (c) distorted output voltage after noise superposition, and (d) corresponding fault classification signal.

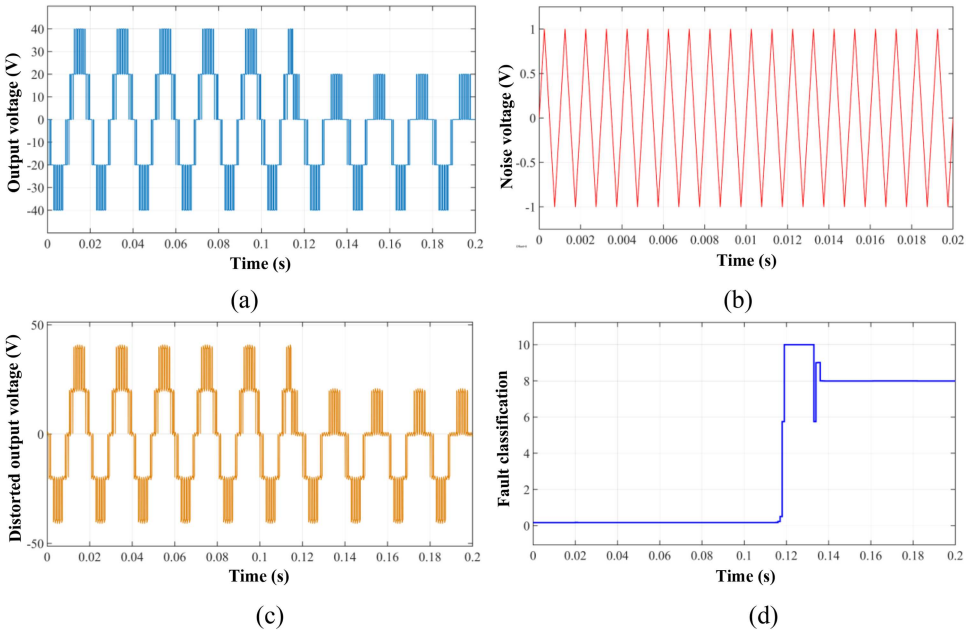

FIGURE 14 | Robustness evaluation under nonsinusoidal noise conditions: (a) original output voltage waveform for Class 8 fault initiated at t = 0.11456 s, (b) injected high-frequency triangular voltage noise (2 V, 1 kHz), (c) distorted output voltage after noise superposition, and (d) corresponding fault classification signal.

by FLS and trigger the fault signal. Figure 9a(iii) shows the FDE alert signal, and FC can be seen in Figure 9a(iv). FLS considers both DF voltage and current for FDE and classification. FLS took 15 ms to detect the fault after OCF was initiated at S_2', and the fault was classified as fault label 6 after 0.13 s. The same analysis can be extended for the remaining fault classes and cases. The findings of fault classes of 6 and 7 are illustrated in Table 6.

4.3 | Performance During Faults of Classes 8–11

In this section, five OCF scenarios are analyzed and categorized into four distinct fault classes, as summarized in Table 7. The first two cases, corresponding to OCFs at switches S_1 and S_3', are grouped under fault Class 8. The remaining three cases, involving faults at S_3S_1', S_3, and $S_1'S_1'$, are classified into fault Classes 9, 10, and 11, respectively. The related waveforms of

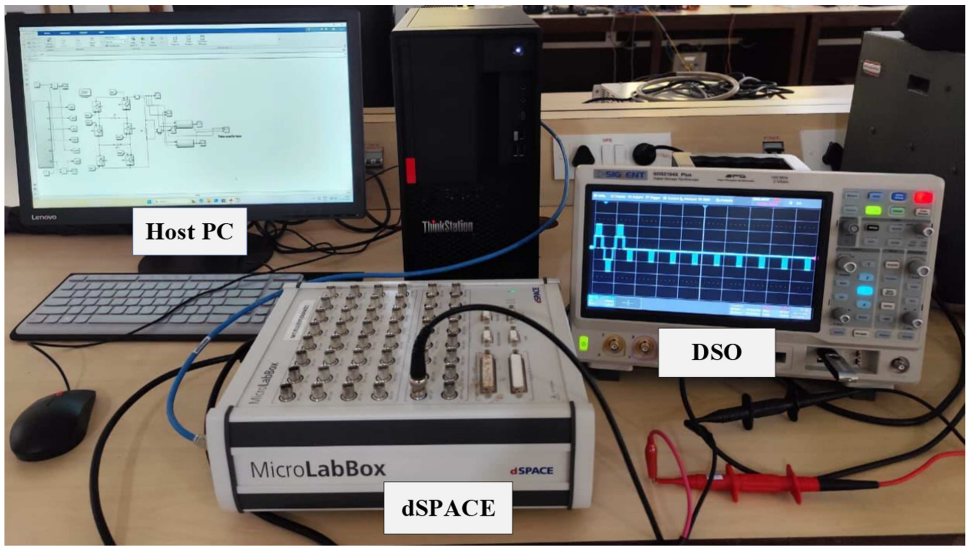

FIGURE 15 | Experimental hardware-in-the-loop test setup. DSO, digital storage oscilloscope; PC, personal computer.

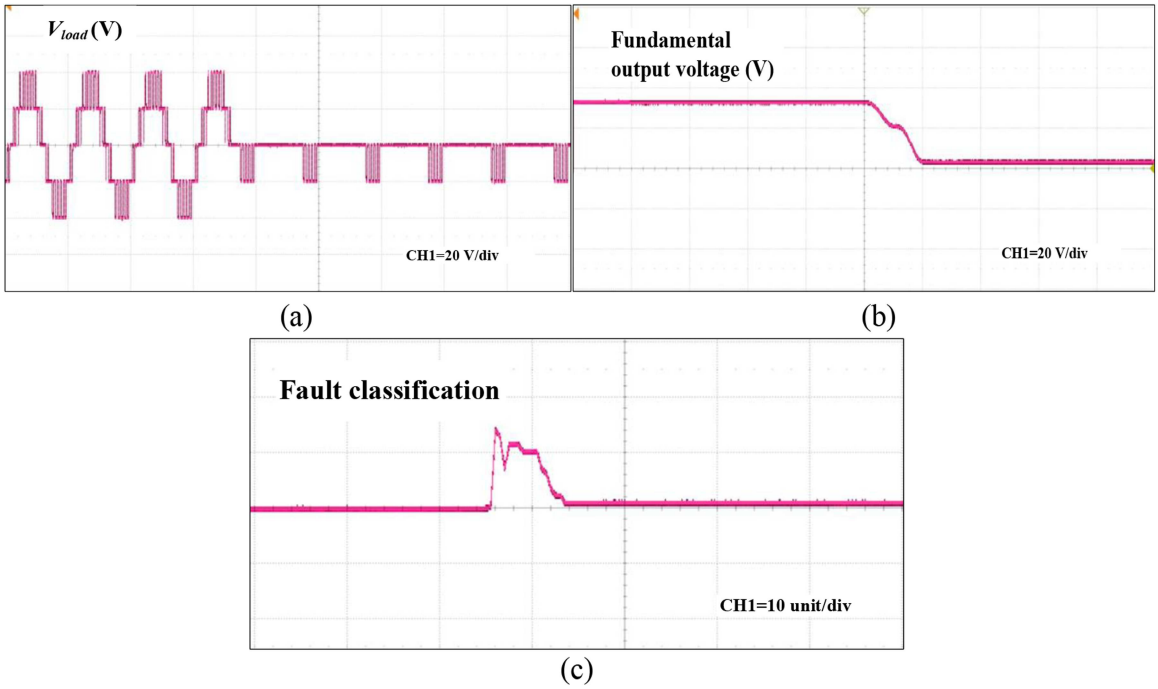

FIGURE 16 | Real-time results: (a) output voltage, (b) fundamental voltage, and (c) fault classification of Class 1 fault.

output voltage, DF voltage, FDE, and FC signals are presented in Figure 10a–d, illustrating the distinct behavioral patterns of each fault condition.

4.4 | Evaluation of the Proposed Diagnostic Model Under Noisy Conditions

To evaluate the robustness of the proposed fuzzy logic-based diagnostic framework under realistic operating conditions, measurement noise is deliberately introduced into the output voltage signal. As shown in Figure 11a, the original inverter output voltage was superimposed with a low-amplitude, high-frequency sinusoidal noise of 1 V at 1 kHz, illustrated in Figure 11b, to simulate sensor noise and switching-related disturbances commonly present in practical inverter environments. The resulting distorted voltage waveform is shown in Figure 11c, and the corresponding FC output (Class 7) is presented in Figure 11d. The noisy voltage signal was processed using the same DFT-based feature extraction and FLS without any modification to the diagnostic rules. Although the output voltage waveform becomes visibly distorted due to noise, the fuzzy classifier relies on the fundamental component extracted using the DFT, which remains unaffected by high-frequency disturbances. Consequently, accurate fault detection and classification are preserved. Similar behavior is observed for other noise conditions, including 2 V at 300 Hz, 1 V at 500 Hz, and 1 V at 2 kHz, where the proposed model consistently identified the correct fault class. In addition, the same robustness analysis is carried out for a Classes 3, 1, and 8 fault scenario, and the corresponding results are presented in Figures 12–14, respectively, further confirming the

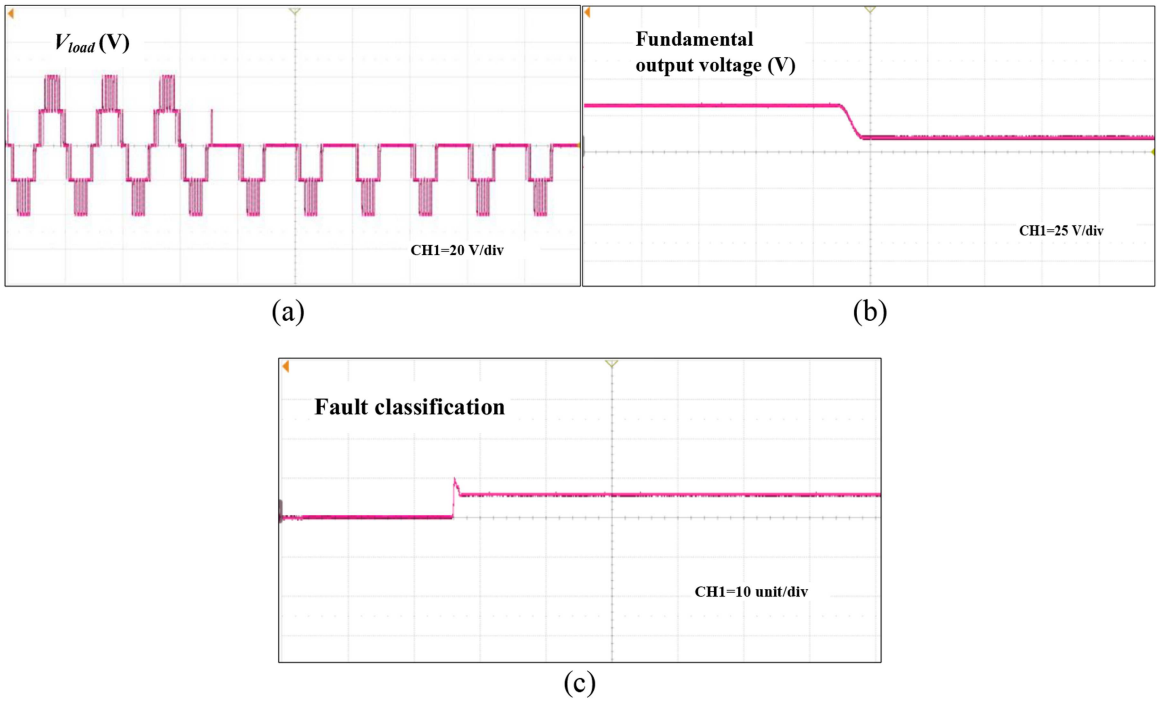

FIGURE 17 | Real-time results: (a) output voltage, (b) fundamental voltage, and (c) fault classification of Class 6 fault.

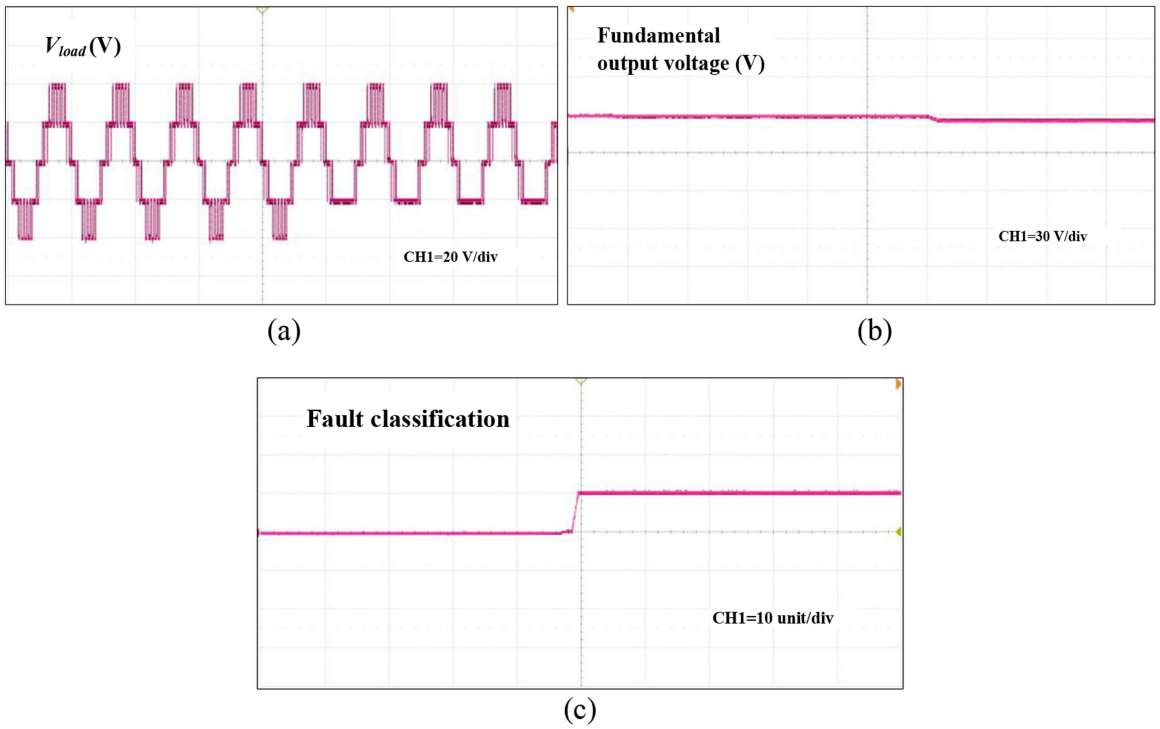

FIGURE 18 | Real-time results: (a) output voltage, (b) fundamental voltage, and (c) fault classification of Class 11 fault.

reliability of the proposed DFT-based fuzzy diagnostic framework under noisy measurement conditions.

4.5 | Experimental Validation

The real-time implementation of the proposed FDE and classification technique for the CCS-MLI using a fuzzy logic framework was carried out on a dSPACE real-time control platform fully integrated with the MATLAB/Simulink environment. The complete Simulink model is automatically translated into real-time executable code through the real-time interface and executed on the dSPACE DS1202 controller. This configuration enabled hardware-in-the-loop (HIL) operation, where all control and FDI algorithms were processed in real time. The control desk software environment enables real-time

TABLE 8 | Impact of fault commencement time for fault classification.

Class	Fault type	Fault mode (OC)	Fault inception angle	Fault inception time (s)	Fault recognition time (ms)	FC time (ms)
1	Two switches	S_2', S_3'	32.73	0.10182	3.18	18.18
2	Two switches	S_1, S_2	65.46	0.10364	1.36	20.36
3	Two switches	S_1, S_3'	98.19	0.10546	2.54	21.54
4	Two switches	S_1', S_2'	130.92	0.10728	6.72	20.72
5	Two switches	S_2, S_3	163.65	0.1091	5.9	19.9
6	Single switch	S_2'	196.38	0.11092	4.08	10.08
7	Single switch	S_2	229.11	0.11274	12.26	17.76
8	Single switch	S_1	261.84	0.11456	3.44	21.44
9	Two switches	S_3, S_1'	294.57	0.11638	10.62	20.62
10	Single switch	S_3	327.3	0.1182	8.8	9.8
11	Single switch	S_1'	360	0.12	8	8.2

Abbreviations: FC, fault classification; OC, open circuit.

monitoring, online parameter tuning, and data acquisition, providing an effective platform for observing and analyzing system performance during operation. The inverter output characteristics were concurrently observed using a digital storage oscilloscope (DSO) to verify the simulation results. Figure 15 shows an experimental test setup using a host PC, dSPACE DS1202 controller, and DSO (SDS2104X Plus). It was experimentally demonstrated that the fuzzy logic-based system effectively identifies and classifies faults occurring across various switch combinations in the CCS-MLI. There are three fault categories selected based on the DF voltage ranges low, medium, and high: Classes 1, 6, and 11 were implemented and validated in real time using the experimental test setup.

The real-time experimental results for these three cases of the fuzzy-based FDI system are shown in Figures 16–18. Figure 16a illustrates the output voltage waveform during a Class 1 fault in the switches $S_2'S_3'$, showing the change in waveform shape before and after the fault occurrence. Once the fault is initiated, a noticeable loss of voltage levels can be observed in the results. Figure 14b presents the change in DF voltage from 33.74 to 4.08 V. Figure 14c presents the FC signal, correctly identifying the occurrence of a Class 1 fault. Similar analysis can be done for Classes 6 and 11 faults, which are presented in Figures 17 and 18. These results demonstrate the effectiveness and robustness of the proposed fuzzy-based FC approach.

4.6 | Impact of Fault Commencement Time

In this section, the performance of the proposed fuzzy-based approach is evaluated for various OCFS occurring at different fault inception times and angles. The findings summarized in Table 8 clearly demonstrate that the system consistently identifies and classifies faults with high precision, irrespective of the instant or angular position at which the fault occurs.

4.7 | Overall Performance Evaluation

Figure 19 presents the confusion matrix corresponding to the fuzzy-based FC model. The confusion matrix serves as a visual evaluation tool that reflects the effectiveness of class identification, indicating both correctly recognized and misclassified categories. The final row and column summarize the accuracy achieved by each class, while the bottom-right cell represents the overall FC performance, accounting for any possible errors. The diagonal cells, highlighted in green, denote correct predictions where the classified outcome matches the actual condition. Ideally, all data points lie along this diagonal, indicating perfect classification with no off-diagonal deviations. In the present study, the fuzzy-based classifier achieved a false positive rate of zero, confirming that all fault categories were identified accurately. As a result, the developed fuzzy logic-based FC framework demonstrated complete accuracy in detecting and recognizing OC faults.

4.8 | Comparative Analysis

To assess the effectiveness of the proposed fuzzy logic-based classification method, a comprehensive comparative analysis

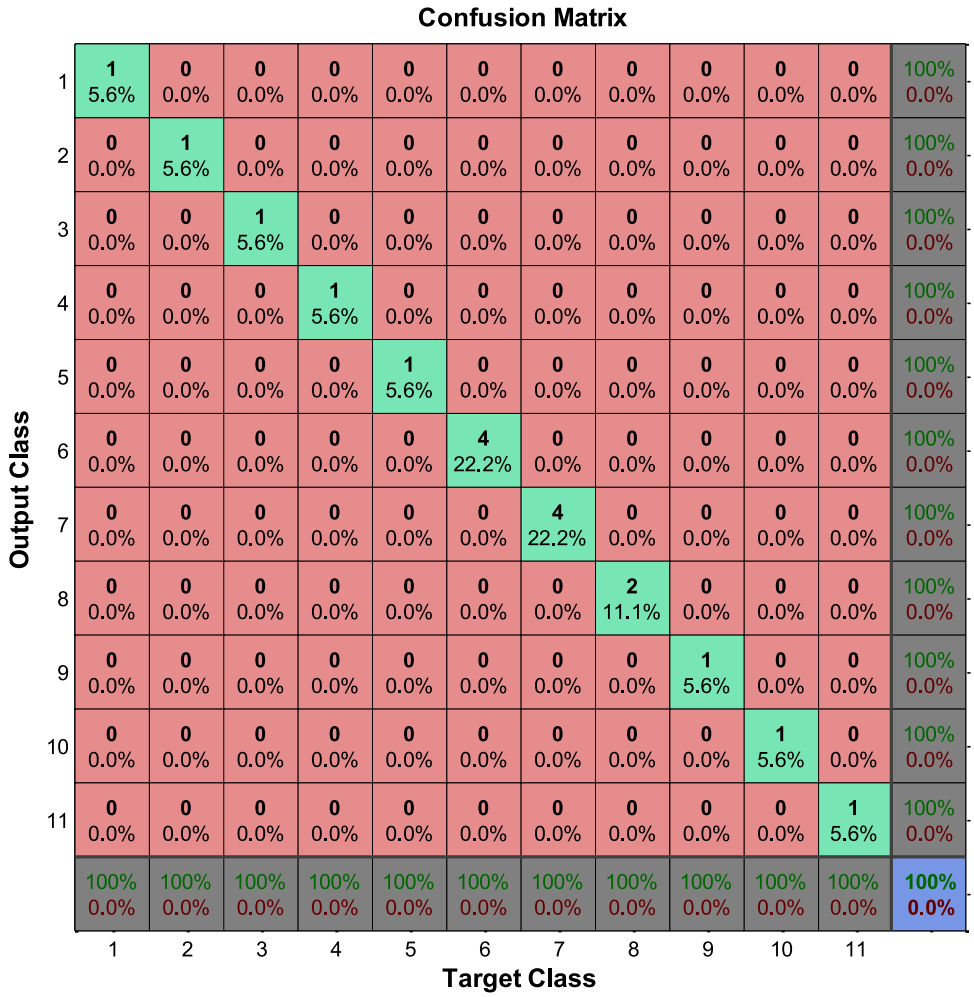

FIGURE 19 | The confusion matrix of the proposed fuzzy logic system.

was performed against several existing diagnostic techniques. The diagnostic approaches summarized in Table 9 are implemented on different converter topologies, voltage levels, diagnostic methodologies, and fault classes, with varying fault diagnosis times and reported accuracies. Therefore, the comparison provides contextual performance benchmarking rather than a strictly identical configuration comparison. Variations in switch count, sensing requirements, feature extraction methods, and data set size may influence the reported accuracy and response times across different studies. Earlier work in [9] employed a model-based FDE approach using a Luenberger observer for DC–DC converters. Although the method proved effective, it offered limited classification capability and did not provide explicit accuracy metrics. ML and DL based schemes reported in [19–23] have achieved classification accuracies between 98.3% and 99.6%, with response times as short as 1.027 ms in CNN-based architectures designed for three-level hybrid active neutral-point-clamped inverters [20]. Despite these promising outcomes, such data-driven models generally demand large volumes of training data, which increases computational cost and processing time. For instance, Hu et al. [19] demonstrated 99.6% accuracy within 20 ms using eXtreme Gradient Boosting for MMCs, while [21] achieved 98.3% accuracy with CNNs applied to CHB-MLIs.

Hybrid diagnostic frameworks, including those presented in [23, 24], have shown improved accuracy but at the expense of higher complexity and computational overhead. The approach in [23] achieved 99.7% accuracy with a response time of 0.33 ms for a three-phase, three-level inverter, whereas [24] reported comparatively lower accuracy (88%–94.12%) for the PUC-5 topology, highlighting the dependence of performance on specific inverter structures.

FLS offer distinct advantages in such contexts due to their low data dependency and simplified computational process. They rely on a set of rule-based inferences rather than extensive training data sets. In [27], a fuzzy-based diagnostic system applied to an MMC achieved FDE within 500 μs but lacked experimental validation. In contrast, Singh et al. [28] successfully implemented a fuzzy system in both simulation and experimental setups for a five-level CHB inverter, achieving 100% accuracy with classification times between 16 and 41.5 ms.

In the present work, a fuzzy logic-based FDE and classification system is developed for the five-level CCS-MLI. The system undergoes verification through simulation and real-time testing using a dSPACE DS1202 HIL platform. The proposed approach effectively detects and classifies OCFs in power switches, achieving 100% classification accuracy with a detection time ranging from 8.2 to 21.54 ms. The algorithm operates at a

TABLE 9 | Comparison with existing methods with respect to OCF classification.

Reference	Converter	Converter voltage level	Diagnosis method	Classification time	Accuracy (%)
[9]	DC–DC converter	—	Model based	Less than two switching periods	Not mentioned
[19]	MMC	9	ML (XGBoost) based	Within 20 ms	99.60
[20]	Hybrid active neutral-point-clamped inverters (HANPC)	3	DL (CNN) based	1.027 ms	99.40
[21]	CHB-MLI	15	DL (CNN) based	Not mentioned	98.30
[22]	Neutral-point-clamped inverter	3	ML based	Not mentioned	99.59
[23]	Three-phase inverter	3	Hybrid approach	Around 0.33 ms	99.70
[24]	Packed U-cell (PUC-5) topology	5	Hybrid approach	Not mentioned	88–94.12
[27]	MMC	5/7	Fuzzy based	Within 500 μs	Not mentioned
[28]	CHB-MLI	5	Fuzzy based	16–41.5 ms	100
Proposed	CCS-MLI	5	Fuzzy based	8.2–21.54 ms	100

Abbreviations: CCS-MLI, cross-connected-source multilevel inverter; CHB-MLI, cascaded H-bridge multilevel inverter; CNN, convolutional neural network; DC, direct current; DL, deep learning; ML, machine learning; MMC, modular multilevel converter; OCF, open-circuit fault; XGBoost, eXtreme Gradient Boosting.

sampling frequency of 100 kHz on the dSPACE DS1202 platform, demonstrating suitability for real-time implementation with low computational overhead. The results confirm high robustness, fast computational response, and strong suitability for real-time operation, making this technique a reliable and efficient alternative to conventional ML, DL, and hybrid diagnostic methods.

5 | Conclusion

This study presents a fuzzy logic-based diagnostic system for detecting and classifying OCFs in CCS-MLI. The fundamental components of the output voltage and current are extracted using the DFT and employed as input features for the FLS. A structured rule base is developed to perform fault detection and classification. The proposed approach demonstrates reliable performance irrespective of fault occurrence time or angular position. Its robustness under realistic operating conditions is verified through deliberate noise injection into the output voltage signal. The results show that accurate fault detection and classification are achieved in approximately one fundamental cycle. Furthermore, real-time HIL simulations confirm the practical applicability of the proposed scheme. A generalized FC framework is also introduced to demonstrate scalability to higher-level MLIs without increasing rule complexity. Comparative analysis highlights the superiority of the proposed method in detecting OCFs, and the approach can be extended to other MLI topologies for FC.

Author Contributions

Niraj Kumar Dewangan: conceptualization, methodology, data curation, formal analysis, validation. **Jeevan N. D.:** data curation, investigation, writing – review and editing, validation. **Krishna Kumar Gupta:** writing – review and editing, writing – original draft, supervision. **Abhinandan Routray:** funding acquisition, writing – original draft, writing – review and editing, data curation, validation. **Hani Vahedi:** writing – review and editing, writing – original draft, visualization, validation.

Acknowledgments

Open access funding is provided by Manipal Academy of Higher Education, Manipal, and agreements with Wiley.

Ethics Statement

Ethical and professional standards have been met. No animals or humans are used in this study.

Conflicts of Interest

The authors declare no conflicts of interest.

Data Availability Statement

The data that support the findings of this study are available from the corresponding author upon reasonable request.

References

1. B. Sharma, S. Manna, V. Saxena, P. K. Raghuvanshi, M. H. Alsharif, and M.-K. Kim, "A Comprehensive Review of Multi-Level Inverters,

Modulation, and Control for Grid-Interfaced Solar PV Systems," *Scientific Reports* 15, no. 1 (2025): 661.

2. A. Poorfakhraei, M. Narimani, and A. Emadi, "A Review of Multilevel Inverter Topologies in Electric Vehicles: Current Status and Future Trends," *IEEE Open Journal of Power Electronics* 2 (2021): 155–170.

3. M. K. Ansari, A. Azeem, A. Sarwar, M. Tariq, and M. R. Hussan, "Control Techniques of Packed U-Cell Multilevel Inverter: A Comprehensive Review," in *Intelligent Computing, Information and Control Systems: ICICCS 2019*, eds. A. P. Pandian, K. Ntalianis, and R. Palanisamy (Springer, 2020), 442–452.

4. M. Trabelsi, H. Vahedi, and H. Abu-Rub, "Review on Single-DC-Source Multilevel Inverters: Topologies, Challenges, Industrial Applications, and Recommendations," *IEEE Open Journal of the Industrial Electronics Society* 2 (2021): 112–127.

5. Z. Chen, M. Yin, J. Yao, G. Liu, Q. Li, and Q. Li, "A Common-Ground Switched-Capacitor Multilevel Inverter With Extended Input Range for Renewable Energy Applications," *International Journal of Electrical Power & Energy Systems* 172 (2025): 111223.

6. V. Aviña-Corral, J. J. Rangel-Magdaleno, J. H. Barron-Zambrano, and S. Rosales-Nuñez, "Review of Fault Detection Techniques in Power Converters: Fault Analysis and Diagnostic Methodologies," *Measurement* 234 (2024): 114864.

7. N. Subramanian and A. A. Stonier, "An Extensive Critique on Intelligent-Based Control Techniques for the Performance Improvement in Multilevel Inverters," *IEEE Access* 13 (2025): 103329–103357.

8. Z. Li, Y. Gao, X. Zhang, B. Wang, and H. Ma, "A Model-Data-Hybrid-Driven Diagnosis Method for Open-Switch Faults in Power Converters," *IEEE Transactions on Power Electronics* 36, no. 5 (2021): 4965–4970.

9. N. Wassinger, E. Penovi, R. G. Retegui, and S. Maestri, "Open-Circuit Fault Identification Method for Interleaved Converters Based on Time-Domain Analysis of the State Observer Residual," *IEEE Transactions on Power Electronics* 34, no. 4 (2019): 3740–3749.

10. K. Xu, H. Wang, and P. X. Liu, "Observer-Based Adaptive Fixed-Time Sensor Fault Compensation Control for Uncertain Nonlinear Systems," *IEEE Transactions on Cybernetics* 55, no. 3 (2025): 1385–1394.

11. I. Jlassi, J. O. Estima, S. K. El Khil, N. M. Bellaaj, and A. J. M. Cardoso, "A Robust Observer-Based Method for IGBTs and Current Sensors Fault Diagnosis in Voltage-Source Inverters of PMSM Drives," *IEEE Transactions on Industry Applications* 53, no. 3 (2017): 2894–2905.

12. X. Zhang, Z. Shang, S. Gao, S. Zhao, C. Chen, and K. Wang, "Open-Circuit Fault Diagnosis for T-Type Three-Level Inverter via Improved Adaptive Threshold Sliding Mode Observer," *Applied Sciences* 15, no. 11 (2025): 6063.

13. C. Shu, C. Ya-Ting, Y. Tian-Jian, and W. Xun, "A Novel Diagnostic Technique for Open-Circuited Faults of Inverters Based on Output Line-to-Line Voltage Model," *IEEE Transactions on Industrial Electronics* 63, no. 7 (2016): 4412–4421.

14. N. Kalaiarasi, A. Sivapriya, P. Vishnuram, M. Bajaj, and A. R. Singh, "Automated Open Circuit Fault Detection in Cascaded H-Bridge Multilevel Inverters Using Artificial Intelligence Technique for EV Application," In *Artificial Intelligence for Integrated Smart Energy Systems in Electric Vehicles. Lecture Notes in Electrical Engineering*, Vol. 1427, ed. S. R. Salkuti (Springer, 2025), https://doi.org/10.1007/978-3-031-94276-1_16.

15. J. Lamb and B. Mirafzal, "Open-Circuit IGBT Fault Detection and Location Isolation for Cascaded Multilevel Converters," *IEEE Transactions on Industrial Electronics* 64, no. 6 (2017): 4846–4856.

16. W. Lang, Y. Hu, C. Gong, X. Zhang, H. Xu, and J. Deng, "Artificial Intelligence-Based Technique for Fault Detection and Diagnosis of EV Motors: A Review," *IEEE Transactions on Transportation Electrification* 8, no. 1 (2022): 384–406.

17. M. U. I. Khan, Md. Ilius Hasan Pathan, M. M. Rahman, et al., "Securing Electric Vehicle Performance: Machine Learning-Driven Fault Detection and Classification," *IEEE Access* 12 (2024): 71566–71584.

18. M. Ali, Z. Din, E. Solomin, K. M. Cheema, A. H. Milyani, and Z. Che, "Open Switch Fault Diagnosis of Cascade H-Bridge Multi-Level Inverter in Distributed Power Generators by Machine Learning Algorithms," *Energy Reports* 7 (2021): 8929–8942.

19. X. Hu, H. Jia, Y. Zhang, and Y. Deng, "An Open-Circuit Faults Diagnosis Method for MMC Based on eXtreme Gradient Boosting," *IEEE Transactions on Industrial Electronics* 70, no. 6 (2023): 6239–6249.

20. S.-H. Kim, D.-Y. Yoo, S.-W. An, Y.-S. Park, J.-W. Lee, and K.-B. Lee, "Fault Detection Method Using a Convolution Neural Network for Hybrid Active Neutral-Point Clamped Inverters," *IEEE Access* 8 (2020): 140632–140642.

21. A. Sivapriya, N. Kalaiarasi, R. Verma, B. Chokkalingam, and J. L. Munda, "Fault Diagnosis of Cascaded Multilevel Inverter Using Multiscale Kernel Convolutional Neural Network," *IEEE Access* 11 (2023): 79513–79530.

22. H. Hu, F. Feng, and T. Wang, "Open-Circuit Fault Diagnosis of NPC Inverter IGBT Based on Independent Component Analysis and Neural Network," *Energy Reports* 6 (2020): 134–143.

23. K. Sarita, S. Kumar, and R. Saket, "OC Fault Diagnosis of Multilevel Inverter Using SVM Technique and Detection Algorithm," *Computers & Electrical Engineering* 96 (2021): 107481.

24. F. A. Khan, M. M. Shees, M. F. Alsharekh, et al., "Open-Circuit Fault Detection in a Multilevel Inverter Using Sub-Band Wavelet Energy," *Electronics* 11, no. 1 (2021): 123.

25. S. Ye, J. Jiang, J. Li, Y. Liu, Z. Zhou, and C. Liu, "Fault Diagnosis and Tolerance Control of Five-Level Nested NPP Converter Using Wavelet Packet and LSTM," *IEEE Transactions on Power Electronics* 35, no. 2 (2020): 1907–1921.

26. S. M. Alapati and V. Singh, "A Novel Approach for Fault Diagnosis of Multilevel Inverter Using DWT and Fuzzy Logic Algorithm," in *2021 2nd International Conference on Smart Electronics and Communication (ICOSEC), Trichy, India* (2021), 1–4, https://doi.org/10.1109/ICOSEC51865.2021.9591900.

27. K. O. M. Touati, I. Merzouk, M. Kheireddine, M. Boudiaf, and A. Hafaifa, "Fuzzy Logic Based Open Circuit Fault Detection and Localization in Modular Multi-Level Converter (MMC)," *Soft Computing* 29 (2025): 5591–5612.

28. V. Singh, A. Yadav, and S. Gupta, "Open Circuit Fault Diagnosis and Fault Classification in Multi-Level Inverter Using Fuzzy Inference System," *Serbian Journal of Electrical Engineering* 20, no. 2 (2023): 163–189.

29. K. K. Gupta and S. Jain, "A Novel Multilevel Inverter Based on Switched DC Sources," *IEEE Transactions on Industrial Electronics* 61, no. 7 (2014): 3269–3278.

30. K. K. Gupta and S. Jain, "A Novel Universal Control Scheme for Multilevel Inverters," in *6th IET International Conference on Power Electronics, Machines and Drives (PEMD 2012), Bristol* (2012), 1–6, https://doi.org/10.1049/cp.2012.0176.